Particle-Scale Simulation of the Flow and Heat Transfer Behaviors in Fluidized Bed with Immersed Tube

Yongzhi Zhao, Maoqiang Jiang, Yanlei Liu, and Jinyang Zheng
State Key Laboratory of Chemical Engineering, Dept. of Chemical and Biochemical Engineering, Zhejiang University, Hangzhou 310027, China

DOI 10.1002/aic.11956
Published online August 25, 2009 in Wiley InterScience (www.interscience.wiley.com).

A kind of new modified computational fluid dynamics-discrete element method (CFD-DEM) method was founded by combining CFD based on unstructured mesh and DEM. The turbulent dense gas–solid two phase flow and the heat transfer in the equipment with complex geometry can be simulated by the programs based on the new method when the k-ε turbulence model and the multiway coupling heat transfer model among particles, walls and gas were employed. The new CFD-DEM coupling method that combining k-ε turbulence model and heat transfer model, was employed to simulate the flow and the heat transfer behaviors in the fluidized bed with an immersed tube. The microscale mechanism of heat transfer in the fluidized bed was explored by the simulation results and the critical factors that influence the heat transfer between the tube and the bed were discussed. The profiles of average solids fraction and heat transfer coefficient between gas-tube and particle-tube around the tube were obtained and the influences of fluidization parameters such as gas velocity and particle diameter on the transfer coefficient were explored by simulations. The computational results agree well with the experiment, which shows that the new CFD-DEM method is feasible and accurate for the simulation of complex gas–solid flow with heat transfer. And this will improve the farther simulation study of the gas–solid two phase flow with chemical reactions in the fluidized bed. © 2009 American Institute of Chemical Engineers *AIChE J,* 55: 3109–3124, 2009

Keywords: fluidized bed, discrete element method (DEM), computational fluid dynamics (CFD), computational granular dynamics (CGD), heat transfer, immersed tube

Introduction

Gas–solid fluidized beds are widely used in the chemical and energy industry to carry out exothermic and endothermic reactions. To control the bed temperature to be a suitable value for reactions, immersed tubes are usually introduced into the fluidized bed. The heat transfer between fluidized bed and immersed body has been a major subject for many investigators because understanding of this process is important for the design of fluidized bed reactors. Although the instantaneous and average heat transfer coefficients of the tube can be obtained by experiment,[1–6] however, the detail of the flow and heat transfer in the bed is still difficult to reveal because the complex interactions among particles, gas and immersed tubes can not be captured easily only by experimental ways. In recent years, with the increase of computational power of computer and the development of computational fluid dynamics (CFD), CFD model and numerical simulation has been an important tool to analyze the fluid dynamics and the heat transfer mechanisms in multiphase

Correspondence concerning this article should be addressed to Yongzhi Zhao at yzzhao@zju.edu.cn or Jinyang Zheng at jyzh@zju.edu.cn

flow. For gas–solid two-phase flow, there are two kinds of mathematical models can be used. One of the commonly used approaches is two-fluid continuum model that represents the gas and solid phases as two interpenetrating continua. Since the kinetic theory for granular flow was founded and introduced into the approach,[7] the prediction precision of the continuum model was enhanced greatly and then the approach was widely employed in the studies of gas–solid two-phase flow. As a basic branch of multiphase flow, the gas–solid fluidization in fluidized bed has also been investigated by the approach. And several investigators have studied the flow behavior in the fluidized bed with immersed tube.[8,9] Schmidt and Renz combined the heat transfer model with the continuum model to study the heat exchange between the fluidized bed and the immersed tube,[8,10,11] but the simulation results are not very quite consistent with the experiments. The possible reason for the inaccurate results is that the two-fluid continuum model is not precise enough caused by the continuity assumption of the solids. For a better understanding of the hydrodynamics and heat transfer mechanisms in fluidized bed, basic physical model including the gas-particle, particle-particle and particle-wall interactions should be fully considered at microscale. However, this becomes a major weakness of the Eulerian–Eulerian two-fluid model. On the contrary, the Eulerian-Lagrangian model is more attractive, in which the particles are traced individually by solving Newton's equations of motion, while the gas phase is treated as a continuum that is coupled to the motion of particles via an interphase interaction term. In modeling the particle motions like molecules, the discrete element method (DEM) received the most emphasis in the literatures.[12] The simulation of fluidized beds using an approach of combining DEM with CFD was pioneered by Tsuji et al.[13] Since then, the method has been widely employed in the simulation of fluidization systems because of its high precision.[14,15] A distinct advantage of the CFD-DEM simulation over the continuum model of fluidized beds is that it has the capability in simulating the microdynamic behavior of granular materials at the individual particle level. In recent years, CFD-DEM has been extended to heat transfer study by a number of investigators. Zhou et al. used the method to model combustion of coal particles in a bubbling fluidized bed, considering the rate of change of the particle internal energy duo to convective heat exchange with surrounding gas, the thermal radiation, the heat of combustion and the interparticle collision heat exchange.[16] Li & Mason adopted the method to model gas–solid two-phase flow with heat transfer in pneumatic transport pipes.[17] Zhou et al. applied the method to study particle–particle and particle-fluid heat transfers in packed and bubbling fluidized beds at an individual particle scale, involving three heat transfer mechanisms: fluid-particle convection, particle–particle conduction and particle radiation.[18] However, so far most CFD-DEM simulations in the published literatures are based on structured CFD grid, and only the systems with simple geometry can be solved. For simulating the multiphase flow in the equipment with complex geometry such as fluidized bed with immersed tube, the traditional CFD-DEM method must be improved. Rong et al. have studied the behavior of particles and bubbles around tubes in fluidized bed by simulation using a modified CFD-DEM method, in which the whole calculation domain was meshed with square fluid cells and the tube boundary was approximated by staircase-like lines for gas flow prediction.[19,20] However, the unrealistic assumption of the tube boundary may reduce the prediction precision of the flow field if the CFD cells are not small enough, so the revised CFD-DEM method is not quite suitable for solving the flow in the equipment with complex geometry. In this article, a kind of new modified CFD-DEM method was founded by combining DEM and CFD based on unstructured mesh. The turbulent dense gas–solid two phase flow and the heat transfer in the equipment with complex geometry can be simulated by the programs based on the new method when the k-ε turbulence model and the multiway coupling heat transfer model among particles, walls and gas were employed. In the present work, the fluidized bed with single immersed tube was simulated by the new method. The microscale mechanism of heat transfer in the fluidized bed was explored by the simulation results and the critical factors that influence the heat transfer between the tube and the bed were discussed.

Mathematical Model

Model of discrete phase

The particle movement is described by the Newton's equation of motion which includes the effects of gravity force, contact force, fluid drag force and buoyant force. For a particle with mass m and moment of inertia I, the equations of translational and rotational motions can be written as

$$m\frac{d\boldsymbol{v}}{dt} = m\boldsymbol{g} + \sum \boldsymbol{F}_{\mathrm{c}} + \boldsymbol{F}_{\mathrm{d}} + \boldsymbol{F}_{\mathrm{b}} \tag{1}$$

$$I\frac{d\boldsymbol{\omega}}{dt} = \sum \boldsymbol{T}_{\mathrm{c}} \tag{2}$$

where the translational motion of the particle is a function of the sum of forces acting on the particle while the rotational motion of the particle depends on the contact torque acting on it. In Eqs. 1 and 2, $d\boldsymbol{v}/dt$ represents the acceleration of the translational motion of the particle and $\boldsymbol{g}$ is the acceleration of gravity, $\boldsymbol{F}_{\mathrm{d}}$ represents drag force, $\boldsymbol{F}_{\mathrm{b}}$ is buoyant force, $d\boldsymbol{\omega}/dt$ represents the acceleration of the rotational motion of the particle. The contact force $\boldsymbol{F}_{\mathrm{c}}$ is composed of the normal contact force $\boldsymbol{F}_{\mathrm{c},n}$ and the tangential contact force $\boldsymbol{F}_{\mathrm{c,t}}$:

$$\boldsymbol{F}_{\mathrm{c}} = \boldsymbol{F}_{\mathrm{c},n} + \boldsymbol{F}_{\mathrm{c,t}} \tag{3}$$

The contact torque $\boldsymbol{T}_{\mathrm{c}}$ considers the torque $\boldsymbol{T}_{\mathrm{t}}$ generated by the tangential contact force and the rolling friction torque $\boldsymbol{T}_{\mathrm{r}}$:

$$\boldsymbol{T}_{\mathrm{c}} = \boldsymbol{T}_{\mathrm{t}} + \boldsymbol{T}_{\mathrm{r}} \tag{4}$$

The contact forces and torques between two spherical particles can be obtained by the three-equation linear spring-dashpot model which was first proposed by Cundall and Strack[12] and improved by Iwashita and Oda.[21] The model estimates the contact forces using the linear spring, dashpot and friction slider, where the parameters of the spring

constants, the damping coefficients and the friction coefficients can be obtained from the physical properties of the particles and the computational conditions.

The normal and tangential contact forces and the rolling friction torque are given by

$$\boldsymbol{F}_{c,n} = -k_n \boldsymbol{\delta}_n - \eta_n \boldsymbol{v}_n \tag{5}$$

$$\boldsymbol{F}_{c,t} = -k_t \boldsymbol{\delta}_t - \eta_t \boldsymbol{v}_t \tag{6}$$

$$\boldsymbol{T}_r = -k_r \boldsymbol{\alpha} - \eta_r \boldsymbol{\omega} \tag{7}$$

where $\boldsymbol{\delta}_n$ and $\boldsymbol{\delta}_t$ are the particle displacements in the normal and tangential directions, respectively, $\boldsymbol{\alpha}$ is the torsional deformation between particles, $\boldsymbol{v}_n$ and $\boldsymbol{v}_t$ are the relative velocities of particles in the normal and tangential directions, respectively, $\boldsymbol{\omega}$ is the relative angular velocity of particles, k the stiffness of the spring and η the coefficient of damping. The damping coefficient can be calculated by the equations in Ref. 22 by using the restitution coefficient. If the following relation is satisfied

$$|\boldsymbol{F}_{c,t}| > f_s |\boldsymbol{F}_{c,n}| \tag{8}$$

$$|\boldsymbol{T}_r| > f_r |\boldsymbol{F}_{c,n}| \tag{9}$$

then the Coulomb friction model is used instead,

$$\boldsymbol{F}_{c,t} = -f_s |\boldsymbol{F}_{c,n}| \boldsymbol{\delta}_t / |\boldsymbol{\delta}_t| \tag{10}$$

$$\boldsymbol{T}_r = -f_r |\boldsymbol{F}_{c,n}| \boldsymbol{\alpha} / |\boldsymbol{\alpha}| \tag{11}$$

where f_s is the sliding friction coefficient and f_r is the rolling friction coefficient.

The torque generated by the tangential force in Eq. 4 can be written as

$$\boldsymbol{T}_t = L\boldsymbol{n} \times \boldsymbol{F}_{c,t} \tag{12}$$

where L is the distance from the center of one particle to the contact plane with the other particle, and $\boldsymbol{n}$ is the normal unit vector.

So far the published literatures about heat transfer in fluidized bed are plentiful, but the study at particle-scale is few. At microscale, the heat in gas–solid fluidized bed can be transferred by the typical three ways: thermal conduction, thermal convection, and thermal radiation. Because the temperature of the system studied in this article is quite low, less than 400°C, the heat transfer by radiation is little and can be ignored, so we can consider that only the thermal conduction and the thermal convection exist in the fluidized bed. According to this, the detail heat transfer forms in the fluidized bed can be obtained by theoretical analysis. They are the heat transfer between particles in contact, between particle and wall in contact, between particle and gas, between gas and gas, and between gas and wall. In above five heat transfer ways, the first three ways are related to the particles. The heat transfer between particles and the heat transfer between particle and wall belong to thermal conduction and that between particle and gas belongs to thermal convection. The equation of the conservation of energy of a particle can be written as

$$mc_p \frac{dT}{dt} = q_{pf} + \sum q_{pp} + \sum q_{pw} \tag{13}$$

where c_p is the specific heat capacity of particle material, T is temperature, t represents time, q_{pf}, q_{pp}, and q_{pw} are the heat transfer flux between the particle and fluid, between the particle and the other particle, and between the particle and the wall, respectively.

The heat transfer between two particles is very complicated and the mathematical model which can accurately describe this process is difficult to found, because the heat transfer flux is related to the deformation between two particles, and the deformation is difficult to calculate correctly. So far several kinds of models have been founded and used to predict the heat transfer in granular materials,[23–27] however the prediction precisions of these models are different. In this article, the model that described in Refs. 25–27 was adopted due to its higher accuracy.[28] The flux of heat transported across the mutual boundary between two particles i and j in contact is written as

$$q_{pp} = H_{pp}(T_{p,j} - T_{p,i}) \tag{14}$$

in which $T_{p,j}$ and $T_{p,i}$ are the temperature of particle j and i, respectively. H_{pp} is the interparticle thermal conductance

$$H_{pp} = 2ak_{pp} \tag{15}$$

where k_{pp} is the thermal conductivity of the solid material and α is the contact radius.

The heat transfer between a particle and a wall in contact is similar to that between two particles, so the flux of heat can be calculated by the same model

$$q_{pw} = H_{pw}(T_w - T_p) \tag{16}$$

in which T_w and T_p represent the temperature of wall and particle, respectively. H_{pw} is the thermal conductance between particle and wall

$$H_{pw} = 2ak_{pw} \tag{17}$$

where k_{pw} is the thermal conductivity between particle and wall (wall material is the same as particle material and so $k_{pw} = k_{pp}$) and α is the contact radius.

Model of continuum phase

The motion of fluid is described by the equation of continuity and the equation of momentum conservation with the local mean variables. The fluid is assumed to be incompressible. The equations are written as follows:

Equation of continuity:

$$\frac{\partial}{\partial t}(\alpha_f \rho_f) + \frac{\partial}{\partial x_j}(\alpha_f \rho_f u_j) = 0 \tag{18}$$

Equation of momentum conservation:

$$\frac{\partial}{\partial t}(\alpha_f \rho_f u_i) + \frac{\partial}{\partial x_j}(\alpha_f \rho_f u_i u_j) = -\frac{\partial p}{\partial x_i} + \frac{\partial}{\partial x_j}\left[\alpha_f \mu_{eff}\left(\frac{\partial u_i}{\partial x_j} + \frac{\partial u_j}{\partial x_i}\right)\right] + \boldsymbol{F}_s \tag{19}$$

where α_f is volume fraction of fluid, u is fluid velocity, ρ_f is fluid density, p is pressure of fluid, x represents coordinates and $\boldsymbol{F}_s$ shows the interaction term due to fluid drag force. The volume fraction of fluid can be calculated by:

$$\alpha_f = 1 - \sum_{i=1}^{n} V_{p,i}/\Delta V \tag{20}$$

where ΔV and $V_{p,i}$ are the volume of a computational cell and the volume of particle i inside this cell, respectively. n is the number of particles in the cell. In present simulations, for two-dimensional flow, we set $\Delta V = \Delta A d_p$, ΔA is the area of a computational cell and d_p is the particle diameter.

In this article, the fluid turbulence is treated with standard k-ε turbulence model. So the fluid effective viscosity μ_{eff} in Eq. 19 is expressed as $\mu_{eff} = \mu + \mu_t$, where μ is the fluid molecular viscosity, μ_t is the fluid turbulent viscosity, $\mu_t = \rho_f c_\mu k^2/\varepsilon$, c_μ is a constant, $c_\mu = 0.09$.

k is the turbulence kinetic energy, and ε is the dissipation rate of the turbulence kinetic energy; they can be obtained from the following equations:

$$\frac{\partial}{\partial t}(\alpha_f \rho_f k) + \frac{\partial}{\partial x_j}(\alpha_f \rho_f u_j k) = \frac{\partial}{\partial x_j}\left[\alpha_f\left(\mu + \frac{\mu_t}{\sigma_k}\right)\frac{\partial k}{\partial x_j}\right] + \alpha_f G_k - \alpha_f \rho_f \varepsilon \tag{21}$$

$$\frac{\partial}{\partial t}(\alpha_f \rho_f \varepsilon) + \frac{\partial}{\partial x_j}(\alpha_f \rho_f u_j \varepsilon) = \frac{\partial}{\partial x_j}\left[\alpha_f\left(\mu + \frac{\mu_t}{\sigma_\varepsilon}\right)\frac{\partial \varepsilon}{\partial x_j}\right] + \alpha_f \frac{\varepsilon}{k} c_1 G_k - \alpha_f c_2 \rho_f \frac{\varepsilon^2}{k} \tag{22}$$

where $G_k = \mu_t S^2$, $S \equiv \sqrt{2S_{ij}S_{ij}}$, $S_{ij} = \frac{1}{2}\left(\frac{\partial u_j}{\partial x_i} + \frac{\partial u_i}{\partial x_j}\right)$. c_1 and c_2 are constants, $c_1 = 1.44$, $c_2 = 1.92$. σ_k and σ_ε are the turbulent Prandtl numbers for k and ε, respectively, $\sigma_k = 1.0$, $\sigma_\varepsilon = 1.3$.

For energy balance, the following equation is derived:

$$\rho_f \frac{\partial(\alpha_f T_f)}{\partial t} + \rho_f \frac{\partial(\alpha_f u_j T_f)}{\partial x_j} = \frac{\partial}{\partial x_j}\left[\left(\alpha_f \frac{k_f}{c_f} + \alpha_f \frac{\mu_t}{\mathrm{Pr}_t}\right)\left(\frac{\partial T_f}{\partial x_j}\right)\right] + Q_{fp} \tag{23}$$

where T_f is the fluid temperature, k_f is the thermal conductivity of the fluid, c_f is the specific heat capacity of the fluid, Q_{fp} is the heat transfer rate between fluid and particles, Pr_t is the turbulent Prandtl number for T_f, which is 0.85 in the present simulations.

Coupling model between two phases

Di Felice[29] proposed a single-function correlation for the drag force on a particle of diameter d_p in a multiparticle system. In this formulation,

$$\boldsymbol{F}_d = \boldsymbol{F}_{d0}\alpha_f^{-(\gamma+1)} \tag{24}$$

where α_f is the porosity around the particle. The fluid drag force on particle in the absence of other particles, $\boldsymbol{F}_{d0}$, and the equation coefficient, γ, are, respectively, given by

$$\boldsymbol{F}_{d0} = \frac{1}{2}\rho_f C_D \frac{\pi d_p^2}{4}\alpha_f^2 |\boldsymbol{u} - \boldsymbol{v}|(\boldsymbol{u} - \boldsymbol{v}) \tag{25}$$

and

$$\gamma = 3.7 - 0.65\exp\left[-\frac{(1.5 - \log_{10}\mathrm{Re}_p)^2}{2}\right] \tag{26}$$

where d_p is the particle diameter, $\boldsymbol{u}$ is the velocity of gas, $\boldsymbol{v}$ is the velocity of particle, C_D is the fluid drag coefficient, and the particle Reynolds number, Re_p, can be expressed respectively as

$$\begin{cases} C_D = \frac{24}{\mathrm{Re}_p} & \mathrm{Re}_p \le 1 \\ C_D = \left[0.63 + \frac{4.8}{\mathrm{Re}_p^{0.5}}\right]^2 & \mathrm{Re}_p > 1 \end{cases} \tag{27}$$

and

$$\mathrm{Re}_p = \frac{\rho_f d_p \alpha_f |\boldsymbol{u} - \boldsymbol{v}|}{\mu} \tag{28}$$

The buoyancy acting on the particle is

$$\boldsymbol{F}_b = \frac{1}{6}\pi d_p^3 \rho_f \boldsymbol{g} \tag{29}$$

As above forces is known for each particle, the volumetric fluid-particle interaction force in a computational cell can be determined by

$$\boldsymbol{F}_s = \frac{-\sum_{i=1}^{n}(\boldsymbol{F}_d^i + \boldsymbol{F}_b^i)}{V_{cell}} \tag{30}$$

where n represents the number of particles in the CFD cell, and V_{cell} is the volume of this CFD cell. This equation reflects the principle of Newton's third law of motion so that the fluid drag force acting on individual particles will react on the fluid from the particles in a computational fluid cell.

For a particle in fluid, the convective heat transfer q_{pf} between gas and particle in Eq. 13 can be calculated by the following equation

$$q_{pf} = \mathrm{Nu}\pi d_p k_f (T_f - T_p) \tag{31}$$

The Nusselt number is estimated by the correlation of Ranz[30]

$$\mathrm{Nu} = 2.0 + 0.6\mathrm{Re}_p^{1/2}\mathrm{Pr}^{1/3} \tag{32}$$

where Pr is the Prandtl number, $\mathrm{Pr} = \mu c_f/k_f$, Re_p is the particle Reynolds number.

Equation 31 is used to determine the heat transfer flux between each particle and the fluid, the volumetric fluid-particle interaction heat flux in a computational cell can be determined by

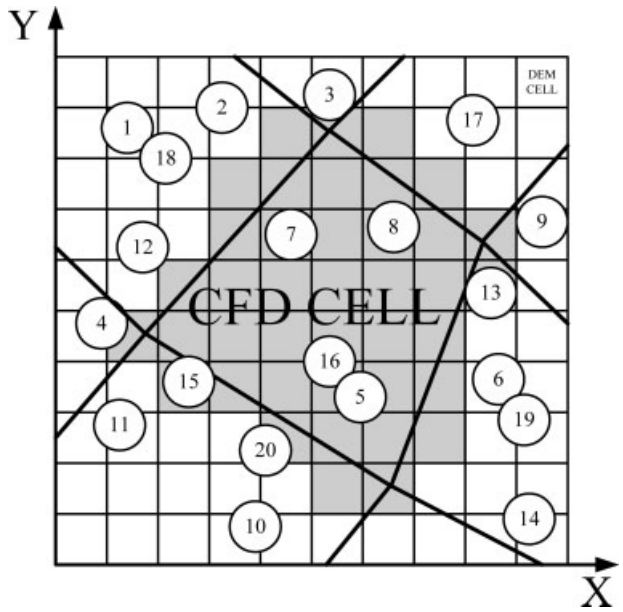

Figure 1. CFD-DEM coupling method based on unstructured mesh.

$$Q_{\mathrm{fp}} = \frac{-\sum_{i=1}^{n} q_{\mathrm{pf}}^{i}}{c_{\mathrm{f}} V_{\mathrm{cell}}} \tag{33}$$

Heat transfer coefficient

The local instantaneous heat transfer coefficient $h(t)$ at any time t and at any point on the tube surface can be written as,

$$h(t) = \frac{q(t)}{A_{\mathrm{tube}}[T_{\mathrm{wall}}(t) - T_{\mathrm{bed}}]} \tag{34}$$

where, $h(t)$ is the local instantaneous heat transfer coefficient, $q(t)$ is the local instantaneous heat flux, A_{tube} is the local surface area, $T_{\mathrm{wall}}(t)$ is the local instantaneous wall (tube surface) temperature and T_{bed} is the near-constant bulk temperature of the bed.

The local instantaneous heat flux $q(t)$ can be divided into two parts, one is the convective heat flux $q_{\mathrm{c}}(t)$ between gas and tube, and the other is the thermal conduction flux $q_{\mathrm{t}}(t)$ between particle and tube:

$$q(t) = q_{\mathrm{c}}(t) + q_{\mathrm{t}}(t) \tag{35}$$

where the convective heat flux $q_{\mathrm{c}}(t)$ between gas and tube is calculated by Newton's law of cooling, and the thermal conduction flux $q_{\mathrm{t}}(t)$ between particle and tube by direct contact is calculated by Eqs. 16, 17. So the heat transfer coefficient between the tube and mediums in the bed can also be divided into two parts, the convective heat transfer between gas and tube, and the thermal conduction between particles and tube. In current research, the two parts of the heat transfer coefficient are obtained respectively by the simulations, and discussed in the section "Results and Discussion".

Solution

In CFD-DEM simulations, search algorithm is the key to control the computational speed of the program. For CFD-DEM simulations with structured rectangular computational fluid cells, there is only one kind search process that is finding neighbors of the particle, controlling the program speed. However, for the simulations of fluidized beds with complex geometric boundary meshed with unstructured computational fluid cells, there are three kinds of searches, which are finding neighbors of the particle, finding neighbors of the wall, and finding particles in the cell. They all control the computational speed. In this research, several kinds of efficient search algorithms were proposed and employed, and the new algorithms greatly enhanced the computational efficiency of the program.

For solving particle motion by discrete element model, the detail computing procedure is that, (1) seeking contacted neighbors of each particle in the granular system, (2) yielding the force and torque acting on each particle using Eqs. 3–12, (3) yielding the particle velocities and new positions using Eqs. 1, 2, (4) return to step 1 for looping. The easiest and original way for finding contacted neighbors of a particle is the straightforward "all–all" calculation. Such a search has an operation count of $O(N^2)$ and is a kind of extremely expensive algorithm, where N is the total number of the particles. As we know, a particle can not contact with all particles in the system at a certain time. A well-known algorithm called linked-cell method proposed by Iwai et al. is introduced here for particle-pair detection.[31] The method divides the computational domain into small rectangular boxes, so-called "cells". Since the search region for each particle is narrowed to cells in the vicinity of the target particle, this method reduces the complexity to $O(N)$. This algorithm avoids the redundant calculations, so it is faster.

For finding particles in the unstructured CFD cell and finding neighboring particles of the wall, a faster search algorithm is not easy to realize. For finding particles in CFD cell, the easiest and direct way is the straightforward "all particles-all CFD cells" calculation. Such a search has an operation count of $O(N{\cdot}M)$ and is a kind of extremely expensive algorithm, where M is the total number of CFD cells. In this article, an efficient method based on linked-cell method was proposed for finding particles in the unstructured CFD cell. In current algorithm, each CFD cell were related with some DEM cells at the program beginning, and then only the particles in the DEM cells related with the CFD cell need to be searched. Since the search region for each CFD cell is narrowed to the DEM cells in the vicinity of the target CFD cell, this method reduces the complexity to $O(M)$. As shown in Figure 1, there are 20 particles and nine CFD cells in the computational domain. The gray rectangles represent the DEM cells that related with the CFD cell at the center of the region. There are seven particles 5, 7, 8, 13, 15, 16, 20 locating in the DEM cells related with the CFD cell. The vectorized distance between a particle and the four boundaries of the CFD cell decides whether the particle is in the CFD cell or not. Calculation results show that the particles 5, 7, 8, 16 are in the CFD cell. The method to find neighboring particles of the wall is similar, and is not described here.

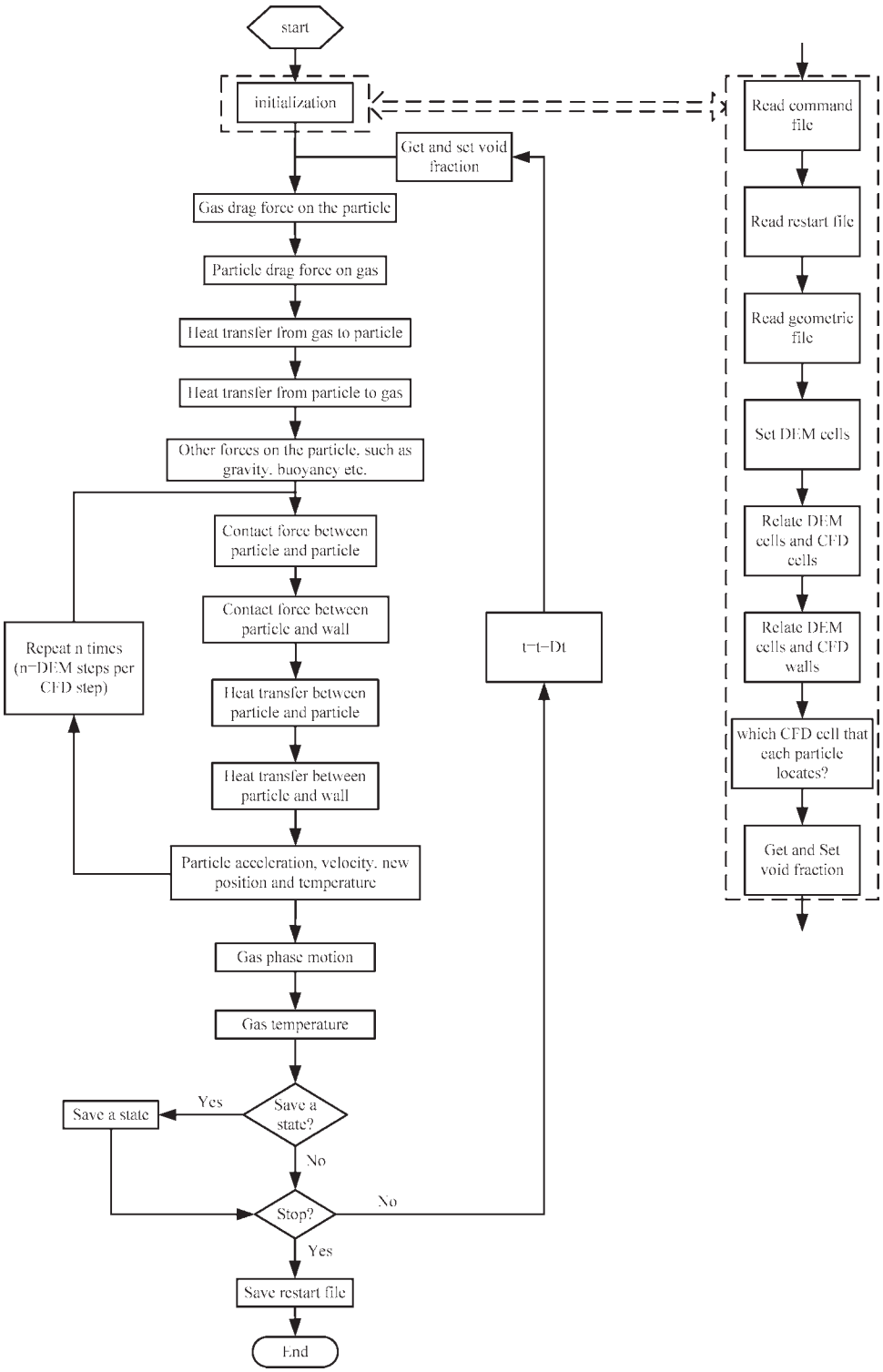

Figure 2. Sketch of the new modified CFD-DEM coupling algorithm.

The calculation flow chart is shown in Figure 2. Although the first step of the program is initialization, much preparing work should be done before the program starts. A command line file that includes simulation parameters (3D or 2D? particle parameters, gravity, etc.) must be set. A restart file that stores the initial information of particles (position, velocity, etc.) and a geometric file that stores the information of CFD cells and walls must be built. When the program starts, the command file, restart file and geometric file are read into memory in turn. And then DEM cells are created by a subroutine, the relationships between DEM cells and CFD cells, CFD walls are built subsequently. Then the void fractions of CFD cells are calculated rapidly by using the new method mentioned above.

Once the system is initialized, for each time step, the drag forces and the heat transfer between particles and gas, the contact forces and heat transfer between particles, and between particles and walls, particle gravity, buoyancy etc. are carried out, and then the acceleration, velocity and the new position of each particle are obtained by the calculation. If there are several DEM steps per CFD step, the contact forces, the new velocities, positions, and heat transfer of particles will be calculated per DEM step. When the calculation of particle motion is completed, the calculation of fluid motion and heat transfer is carried out, and then a cycle is completed. During the calculation, the current velocities, positions and temperatures of particles and the gas velocity, temperature and pressure fields can be saved by a command called "Save a state". The sequence can be ended by a "stop" command and a restart file will be saved before the end.

For CFD solution, the present study uses a control volume formulation, details of which are in Patankar's literature.[32] The governing equations are discretized in finite volume form by unstructured mesh. The SIMPLEC method[33] is used to solve the equations for the fluid phase in the continuum model. The third-order QUICK differencing scheme[34] is used for the convective terms and the first-order implicit time integration method is used to solve the motion of fluid. For DEM solution, the explicit time integration method is used to solve the translational and rotational motions of particles.[12]

Simulation conditions

In the continuum model, the no-slip boundary condition was applied to the bed walls and zero diffusion flux condition to the top exit. At the bottom of the beds, the gas velocity introduced was uniform. In the discrete element model, the interparticle force model was also applied to the collision between the particles and the wall, and the contact forces could be calculated from the displacements between every particles and walls. We started by randomly putting particles into the bed. The particles fell due to gravity, and lost their energy due to dissipation when they contacted with bed walls and other particles. After a period of time they were packed in the bed with no significant motion, then the gas was introduced and simulations were beginning.

The simulation parameters are given in Table 1. According to Ting and Corkum's suggestion, the value of damping coefficient was derived from the coefficient of restitution.[22] The critical time step for particle motion is determined by the following equation:

$$\Delta t = \frac{1}{10} T_s \tag{36}$$

where T_s is the oscillation period of the spring-mass system. The time step employed in simulations must be shorter than the critical time step.

The structure and CFD grids of the fluidized bed simulated in this article are two-dimensional, shown in Figure 3. The height and the width of the bed are 750 mm and 150 mm respectively, and the diameter of the immersed tube is 40 mm. The temperature of the tube is set to be constant, 373 K, and the bed wall is set to be adiabatic. The fluidization gas is air and the temperature of the gas is set to be 273 K. The material of the particle in the simulations is glass and the density is 2600 kg m^{-3}. The initial temperatures of the particles and the air in the bed are same, 273 K. The detail of the simulation parameters can be seen in Table 1. In the simulations, three kinds of particles with diameters, 0.5 mm, 1.0 mm, 1.5 mm, were employed in different cases to explore the influence of particle size on heat transfer, and the number of particles in each case is 68,400, 17,100, and 7600, respectively to ensure the initial bed heights are same. The maximum of the three minimum fluidizing velocities (u_{mf}) is 0.90 m s^{-1} calculated by Ergun equation,[35] and consequently, the minimum velocity of the gas at the inlet is set to be 1.2 m s^{-1}. For investigating the influence of gas velocity on heat transfer, the speeds of the gas at the inlet are also set to be 1.2 m s^{-1}, 1.6 m s^{-1}, 2.0 m s^{-1} in different simulation cases. In this article, five cases of fluidized bed with an immersed tube were simulated by using the new method, the different setting of parameters is shown in Table 2. In all cases, the CFD time step is 5×10^{-5} s, and the DEM time step is 5×10^{-6} s, which is shorter than the critical time step calculated by Eq. 36.

Table 1. Parameters Used in the Simulations

Parameters	Value
Gas properties	
Density/kg m^{-3}	1.225
Viscosity/N s m^{-2}	1.72×10^{-5}
Thermal conductivity/W m^{-1} K^{-1}	0.0242
Specific heat/J kg^{-1} K^{-1}	1006
Particle properties	
Diameter/mm	0.5, 1, 1.5
Density/kg m^{-3}	2600
Coefficient of restitution	0.9
Coefficient of sliding friction	0.3
Coefficient of rolling friction/m	0.00005
Thermal conductivity/W m^{-1} K^{-1}	0.77
Specific heat/J kg^{-1} K^{-1}	800
Simulation parameters	
Number of particles	68,400, 17,100, 7600
DEM time step/s	5×10^{-6}
CFD time step/s	5×10^{-5}
Total simulation time/s	20
Gas inlet velocity/m s^{-1}	1.2, 1.6, 2.0
Gas inlet temperature/K	273

Results and Discussion

The total simulation time in all five cases is 20 s. A stable fluidization state can be obtained after a few seconds. According to the simulation results, the fluidization state is unsteady before 10 s, and becomes steady after 10 s. So the calculation results after 10 s can be used to analyze. Figure 4 shows the instantaneous images of solids concentration and gas velocity vectors in the fluidized bed with different superficial gas velocities of 1.2, 1.6, and 2.0 m s^{-1}, respectively. The diameter of particles in the three cases is 1.0 mm. Arrows in the figure indicate gas movement and the black dots represent particles. The flow pattern in the fluidized bed with immersed tubes is quite different with that without internals because of the tubes. As can be seen, when a larger bubble is passing by the immersed tube, particles with high speed at the front edge of the bubble will collide

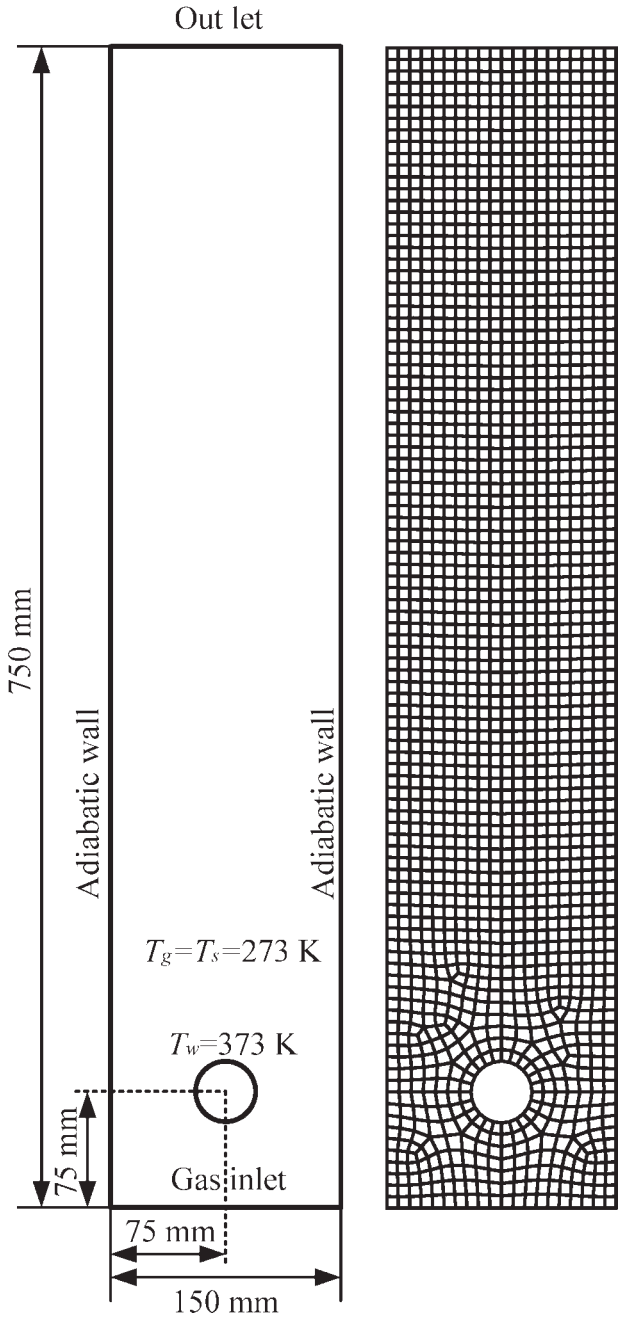

Figure 3. Fluidized bed and CFD mesh.

with the tube and then rebound due to elastic force. As a result, a halo-like cluster is created in the lower side of the tube. At the same time, particles at the right and left sides of the tube still move forward with high-speed and a large air pocket will be formed at the back side of the tube downstream. When the bubble arrives at the top of the bed, it will burst to be disappeared and the particles will then begin to fall down by gravity. When these particles fall around the tube, a large air pocket also will be formed below the tube. The flow pattern shows "cap" of solids above the tube and gas pocket below, which can be found in the experimental studies.[36,37] From the simulation results it can be found that the collision between particles and tubes makes the gas–solid two-phase flow in the fluidized bed more complex. The tube is surrounded by air pockets in the most of the time, and this may greatly prevent the heat transfer between the tube and particles.

As we know, superficial gas velocity has a great effect on the fluidization behavior in the fluidized bed. By comparing the three cases in Figure 4, it can be seen that concentration phenomenon of particles is serious when the superficial gas velocity is low. With gas velocity increasing, gas–solid motion is more and more disordered, and particles are more and more dispersed in the fluidized bed. The flow patterns in the bed are different when the gas velocities are different and this will greatly impact the heat transfer efficiency of the immersed tube, which will be described in detail in the following text.

To explore the heat transfer mechanism and the heat transfer efficiency of the tube in the bed, local instantaneous solid fractions and heat transfer coefficients at different angular locations around the tube were recorded during the simulations. The data at five different angular locations around the tube of Case 1 are shown in Figure 5. Figure 5a shows the variation of local instantaneous solids fraction with time. It can be seen that it exhibits higher value at the top of the tube surface (7.5°), closes to 0.6 most of the time and has a large fluctuation once in a while. That is to say in the most of the time there exist particles concentration on top of the tube. At the position 52.5°, the solids fraction remains high and much of the time closes to 0.6. But the large fluctuation appears more frequent than that at the position 7.5°. This shows that at this location of the tube there are still many particles concentrating near the tube surface, but they will be often blown away by the strong gas flow. And the large fluctuation of the solids fraction is further drastic at the position 97.5° near the middle of the tube. However, at position 142.5° and 187.5°, the solids fraction exhibits very low in the most of the time and occasionally increases to some extent. Obviously, these parts of the tube are surrounded by air pocket most of the time. From the above analysis, the flow pattern in Case 1 can be obtained: because of the lower superficial gas velocity, many particles are retarded and concentrated at the top of the tube, so the solids fraction is high. Whereas, at the right and left sides of the tube, there is higher oscillation of the solids fraction, due to particle clusters shuttling up and down. And below the tube, particle clusters driven by high-speed airflow collide frequently with the tube surface and then rebound due to elastic force. As a result, air pockets are formed below the tube most of the time, so the solid volume fraction below the tube is generally low. The flow pattern described in above text is basically in accordance with the image from Figure 4a.

Table 2. Simulation Parameters of Five Cases

Parameter	Case 1	Case 2	Case 3	Case 4	Case 5
Particle diameter/mm	1.0	1.0	1.0	1.5	0.5
Minimum fluidization velocity/m s^{-1}	0.62	0.62	0.62	0.90	0.24
Gas inlet velocity/m s^{-1}	1.2	1.6	2.0	1.2	1.2
Number of particles	17,100	17,100	17,100	7600	68,400

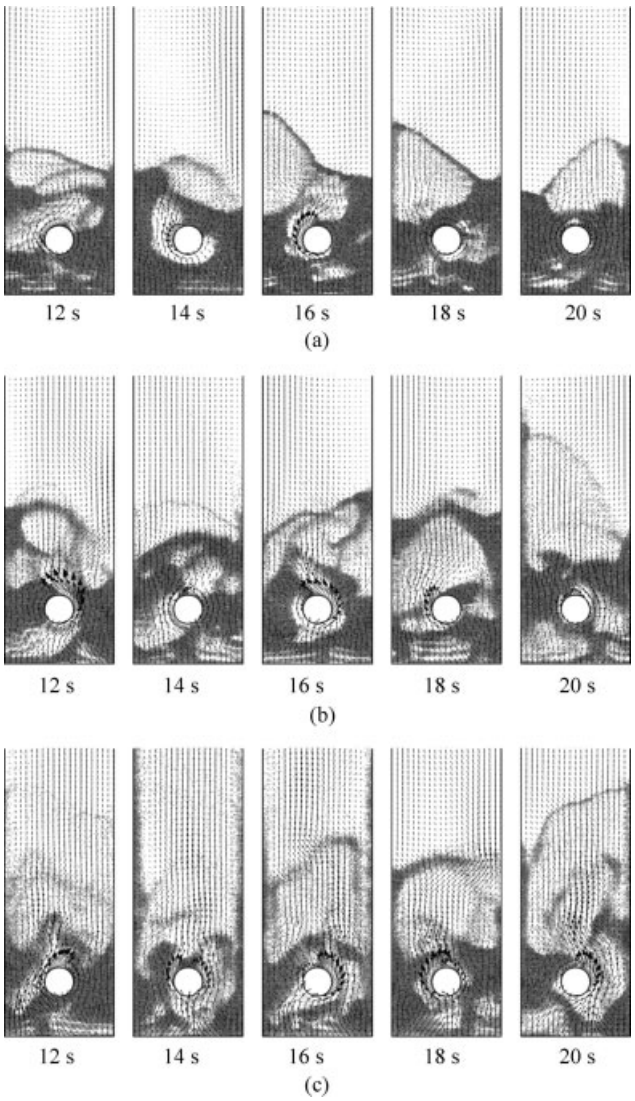

Figure 4. Snapshots of the behavior of gas and solids (d_p = 1 mm, u_{mf} = 0.62 m s^{-1}) in fluidized bed with different superficial gas velocities: (a) v = 1.2 m s^{-1}, (b) v = 1.6 m s^{-1}, (c) v = 2.0 m s^{-1}.

There are two parts of heat transfer between the immersed tube and mediums in the bed, i.e. convective heat transfer between gas and tube, and thermal conduction between particles and tube. Figure 5b represents the variation of the local instantaneous convective heat transfer coefficient between gas and tube with time. It can be seen that the value is fluctuating, and the fluctuations are significantly different at different locations around the tube. For example, it is relatively steady at the top of the tube, whereas, it fluctuates violently at the right and left sides of the tube, though with a low frequency. Yet at the bottom of the tube, it fluctuates slightly, but with a high frequency. Above simulation results are in qualitative agreement with the experimental results in the literature.[4] The main factor affecting the heat transfer coefficients at different angular positions around the tube is the gas–solid motion pattern, which will be described in detail in the following text. Different from the thermal convection between gas and tube, the heat transfer between the tube and particles caused by thermal conduction is directly related to the solids fraction around the tube. Figure 5c shows the local instantaneous heat transfer coefficients between particle and tube caused by thermal conduction. It can be seen that heat exchange exists in the most of the time between particles and the tube at position 7.5° due to particles concentrating at this position. With the position moving down, the total heat exchange time between the tube and

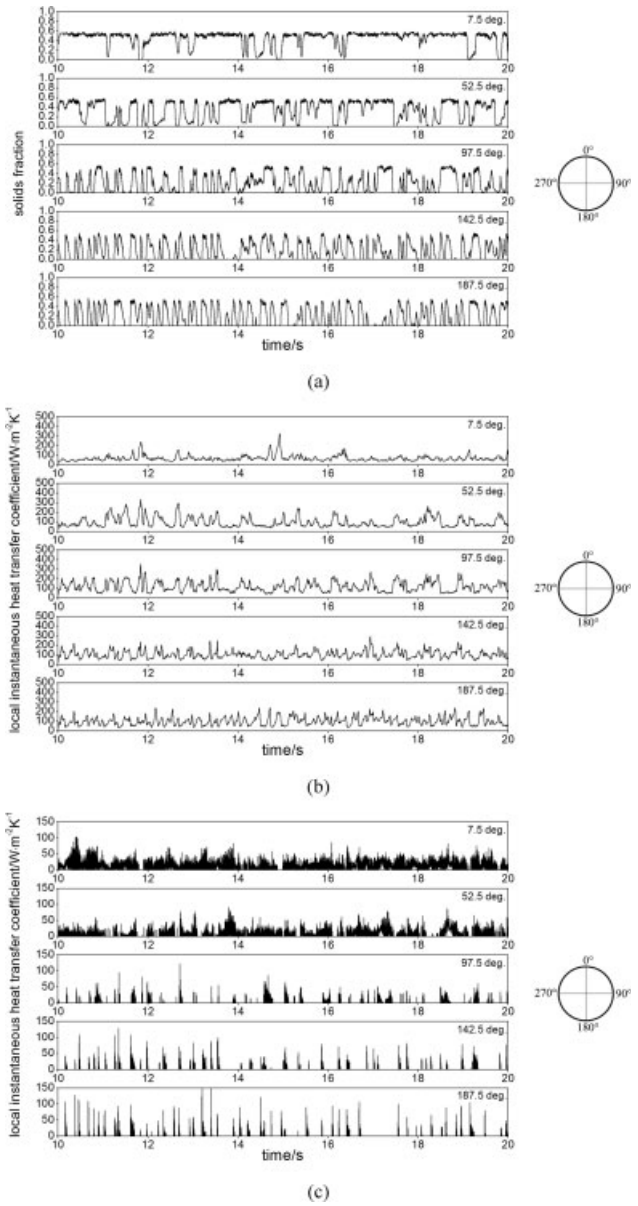

Figure 5. Local instantaneous solids fraction and heat transfer coefficient at the different position around the tube in the fluidized bed (u_f = 1.2 m/s, d_p = 1 mm, u_{mf} = 0.62 m s^{-1}): (a) solids fraction, (b) heat transfer coefficient between gas and tube, (c) heat transfer coefficient between particle and tube.

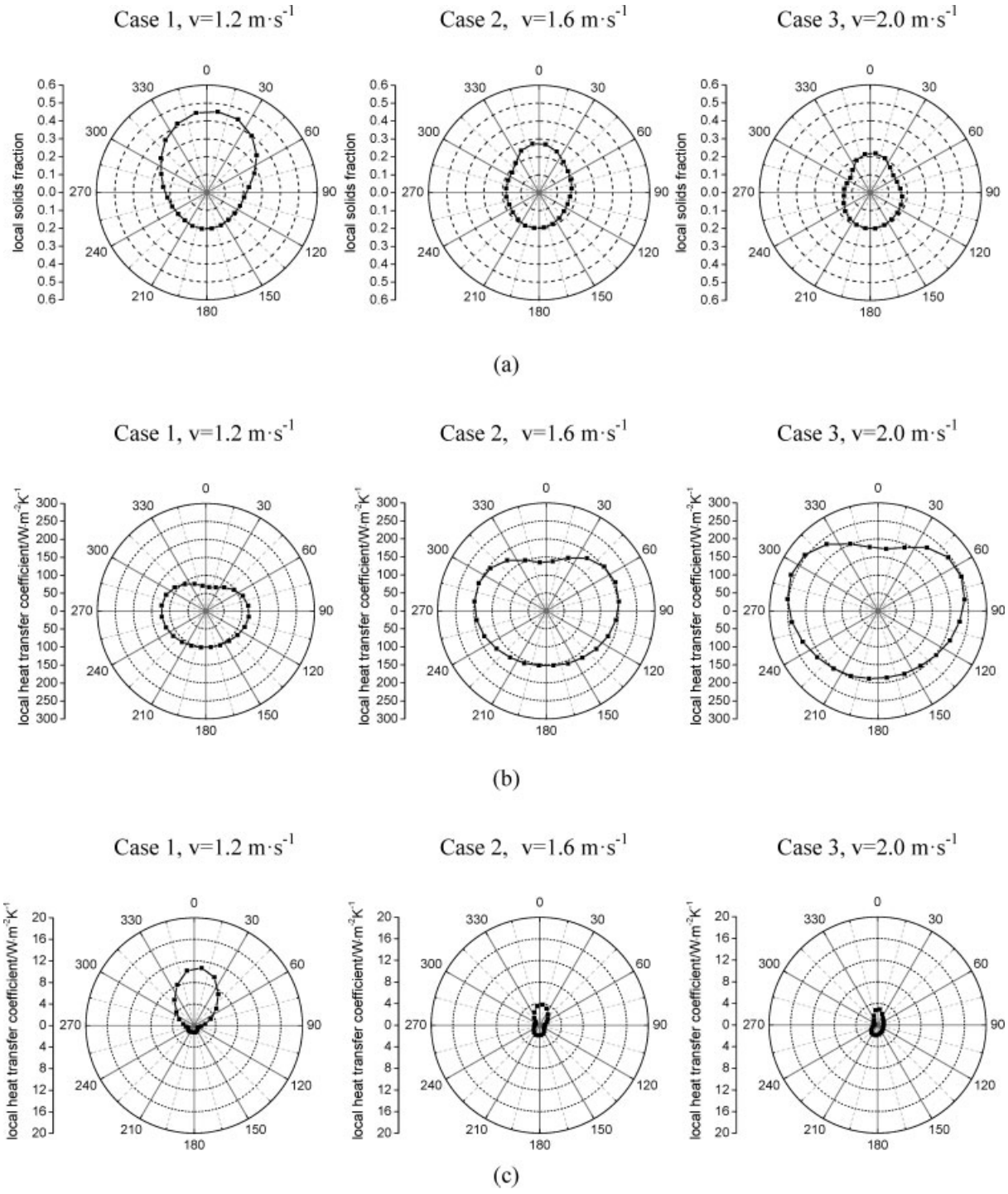

Figure 6. Time averaged local solids fraction and heat transfer coefficient around the tube in the fluidized bed with different superficial gas velocities (d_p = 1 mm, u_{mf} = 0.62 m s^{-1}): (a) solids fraction, (b) heat transfer coefficient between gas and tube, (c) heat transfer coefficient between particle and tube.

particles is gradually decreasing. Especially in the bottom region of the tube, heat exchange is seldom. The reason is that this region of the tube was surrounded by air pockets most of the time. Only when collisions between the particles and the tube surface occur will there be heat exchange. And due to the high contact speed of the particles at the lower position of the tube, the contact area is larger by the strong instantaneous contact force. As a result, the instantaneous heat transfer coefficient at this location is very high when particles contact with the tube.

To systematically study the heat transfer efficiency of the immersed tube in the fluidized bed, the instantaneous data is time-averaged. Figure 6 shows the time-averaged solid volume fraction and heat transfer coefficient around the tube in

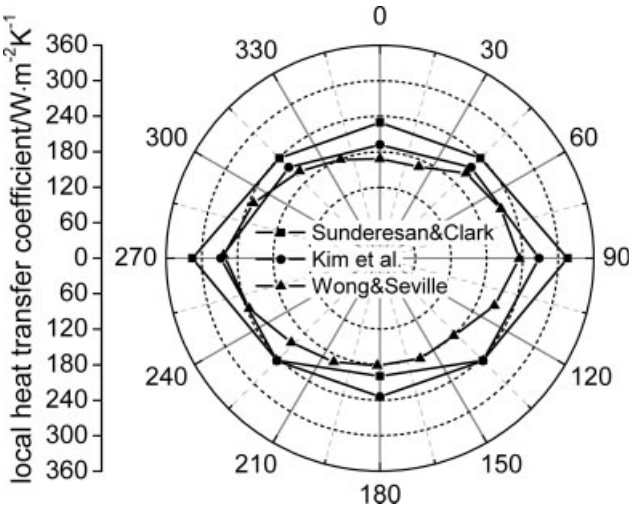

Figure 7. Local heat transfer coefficient around the tube in the fluidized bed by experiments.[4,5,6]

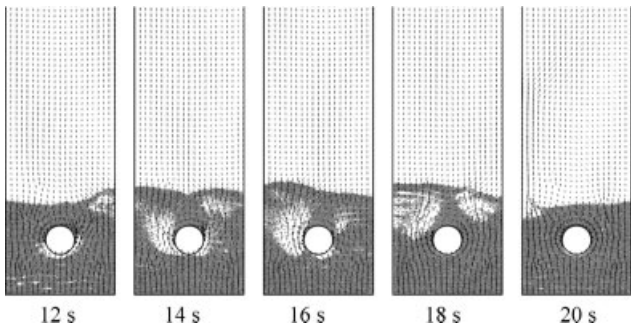

Figure 8. Snapshots of the behavior of gas and solids (d_p = 1.5 mm, u_{mf} = 0.90 m s^{-1}) in fluidized bed with u_f = 1.2 m s^{-1}.

the fluidized bed at different superficial gas velocities. And Figure 6a presents the solids fraction around the immersed tube. It can be seen that the solids fraction at the top of the tube is twice higher than that at the bottom of the tube in Case 1. The value at the top of the tube is 0.45, but at the bottom of the tube is only 0.2, which means that many particles are concentrating at the top of the tube. As the superficial gas velocity is 1.6 m s^{-1}, at the top of the tube, the solids fraction value decreases significantly and the maximum is less than 0.3, as shown in the Case 2 in Figure 6a. However, at the bottom of the tube, its value is almost constant, ~0.2. But at the right and left sides of the tube its value decreases significantly, being less than 0.2. When the superficial gas velocity raises to 2.0 m s^{-1}, at the top of the tube the solid volume fraction further decreases and the maximum reduces to be about 0.2, as indicated in the Case 3 in Figure 6a. But at the bottom of the tube the value has still no obvious change. At the right and left sides of the tube it further decreases, and the minimal value of solid fraction locates at the right and left sides of the tube. From the above analysis, it can be concluded that with the increase of the superficial gas velocity, the reduction of the solids fraction is significant at the top and the right and left sides of the tube, but not obvious at the bottom of the tube. When the gas velocity is low, the minimal value of the solids fraction locates at the bottom of the tube. But as the gas velocity increases, the position gradually moves up to the right and left sides of the tube.

Distributions of time-averaged heat transfer coefficient between gas and tube caused by convection around the tube are shown in Figure 6b. It can be seen obviously that the curve shapes are basically same at different gas superficial velocities and all are similar to ellipse. The maximum of the coefficient locates at the right and left sides of the tube (near 75 and 285°), and the minimum locates at the top or the bottom of the tube (0 and 180°). The minimum is 70–80% of the maximal value. This distribution of the coefficient around the immersed tube is related with the gas–solid flow patterns in the fluidized bed. At the top of the tube, the solids concentration is relatively higher, and high-speed airflow from the bottom of the fluidized bed is obstructed by the immersed tube, so the local heat transfer efficiency between the top surface of the tube and gas is low. At the bottom of the tube, the tube surface is surrounded by air pockets most of the time, and the gas velocity at this point is low since a stagnation point of upstream is formed here, so the heat transfer efficiency between the bottom surface of the tube and gas is low too. However, at the left and right sides of the tube, the gas velocity is relatively higher and a large number of particles shuttle up and down. They can remove heat near the tube, so the heat transfer coefficient is

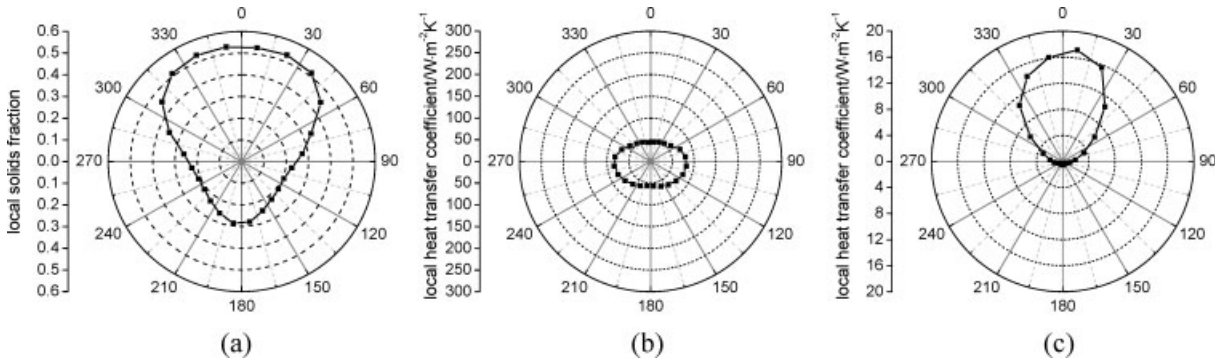

Figure 9. Time averaged local solids fraction and heat transfer coefficient around the tube in the fluidized bed with u_f = 1.2 m s^{-1} and d_p = 1.5 mm: (a) solids fraction, (b) heat transfer coefficient between gas and tube, (c) heat transfer coefficient between particle and tube.

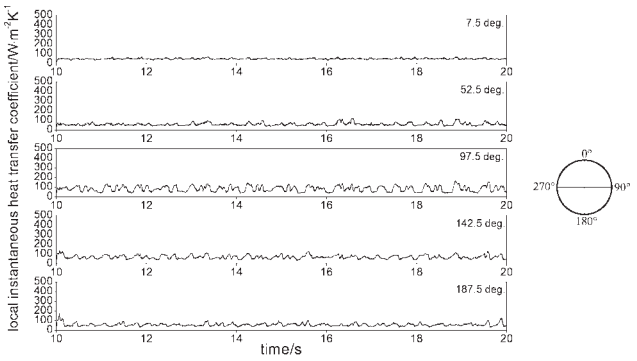

Figure 10. Local instantaneous heat transfer coefficient between gas and tube at the different position around the tube in the fluidized bed (u_f = 1.2 m s^{-1}, d_p = 1.5 mm, u_{mf} = 0.90 m s^{-1}).

relatively higher at the left and right sides of the tube. By comparing three cases in Figure 6b, it can be found that the superficial gas velocity has a great effect on the heat transfer coefficient between gas and tube in the fluidized bed. With the superficial gas velocity increasing, the heat transfer coefficient increases greatly, because increasing the gas velocity around the tube would strengthen the gas turbulence near the tube, and greatly enhance the convective heat transfer between gas and tube.

Different from the thermal convection between gas and tube, the direct contact heat transfer between particles and tube is mainly related to particle concentration. The thermal conduction between particle and tube is directly dependent on their contact time, so high solids concentration around the tube will cause high heat transfer coefficient because of the longer contact time. Figure 6c shows the distribution of heat transfer coefficient caused by heat conduction around the tube. Compared with the Figure 6a, it can be seen that there are many similarities between them in the variation trend of the curves. But the direct contact heat transfer quantity between particle and tube is much smaller than the convective heat transfer quantity between gas and tube. Whereas Comparing Figure 6c with 6b, it can be found that the value difference between them is so large that the direct contact heat transfer quantity between particle and tube can be neglected. The total heat transfer between the tube and mediums in the bed is mainly completed by fluid convection (heat transfer way: tube surface → gas boundary layer near the surface → [by gas motion] → external gas and particles in the bed) and particle convection (heat transfer way: tube surface → gas boundary layer near the surface → particles → [by particles motion] → external gas and particles in the bed). In addition, the direct contact heat transfer rate between particle and tube is closely related to granular materials. In the present simulation, the granular material is glass and the thermal conductivity of glass was 0.77 W m^{-1} K^{-1}, which is very low. If the granular material in the bed is metal which have good thermal conductivity, such as aluminum whose thermal conductivity is 200 W m^{-1} K^{-1}, the direct contact heat transfer between particle and tube will be greatly enhanced, and may be as important as the convective heat transfer between gas and tube and can not be ignored. By comparing three cases in Figure 6c, it can be found that superficial gas velocity also has a great effect on thermal conduction of particle-tube in fluidized bed. The value of thermal conduction decreases with the superficial gas velocity increasing, because the probability and duration time of the contact between particles and tube surface is reduced, due to the increasing expansion ratio of bed and the greatly decreasing of solids fraction around the tube when the gas velocity increases.

So far, two-fluid CFD model has been employed to study the hydrodynamics of gas–solid flow and heat transfer behavior in the fluidized bed with immersed tube, and the time-averaged local heat transfer coefficient around the tube were obtained.[8,10,11] The simulation results show that the maximum of the heat transfer coefficient locates the top of the tube, then the bottom of the tube, and the minimum locates the left and right sides of the tube. However, due to the disadvantages of the two-fluid CFD model, the calculated results are not in agreement well with the experimental data.

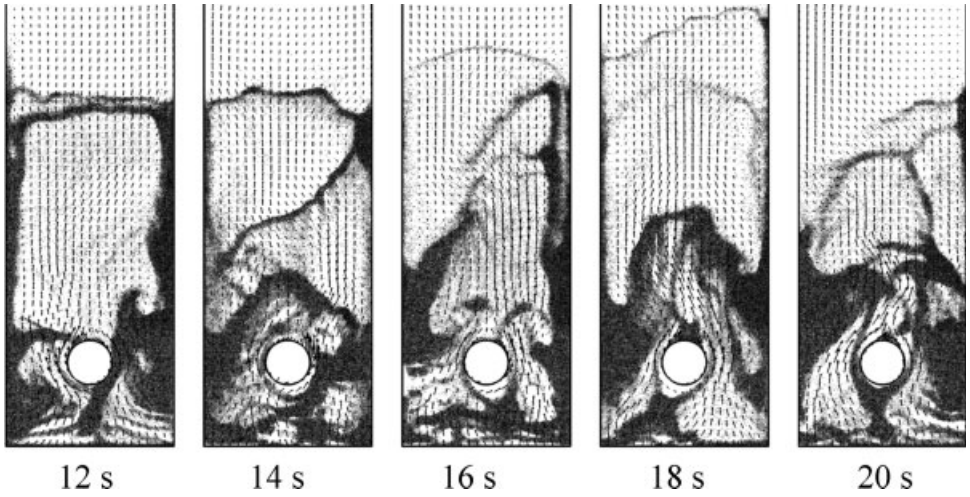

Figure 11. Snapshots of the behavior of gas and solids (d_p = 0.5 mm, u_{mf} = 0.24 m s^{-1}) in fluidized bed with u_f = 1.2 m s^{-1}.

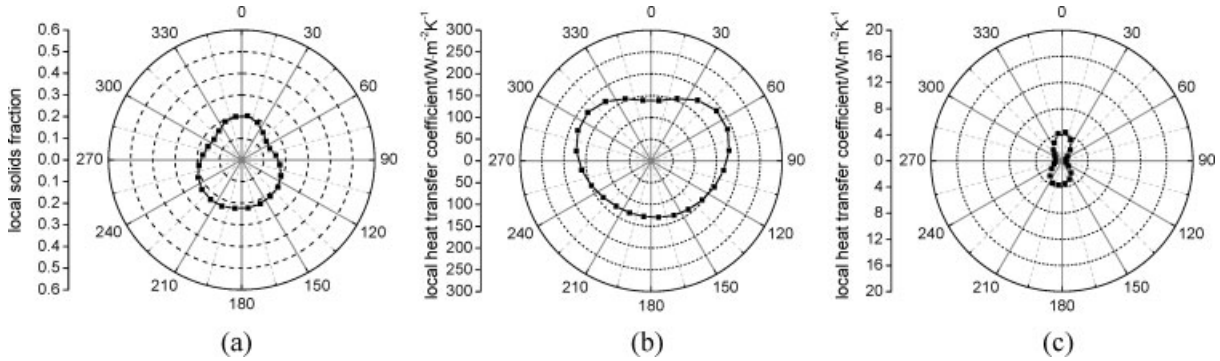

Figure 12. Time averaged local solids fraction and heat transfer coefficient around the tube in the fluidized bed with u_f = 1.2 m s^{-1} and d_p = 0.5 mm: (a) solids fraction, (b) heat transfer coefficient between gas and tube, (c) heat transfer coefficient between particle and tube.

Figure 7 shows the classical distribution of time-averaged heat transfer coefficient around the tube obtained by the experiments.[4,5,6] It can be seen that the value is low at the top and bottom of the tube, high at the left and right sides, and the minimum is 70–80% of the maximum. Compared with the simulation results in literatures,[8,10,11] the present simulation results agree well with the experimental data. This shows that the model established in this article can accurately describe the heat transfer behavior in the fluidized bed.

The factors that affect the heat transfer efficiency between the immersed tube and the fluidized bed are much more, and the size of particles is one important factor of them. To investigate the influence of particle size on heat transfer, other two different particle sizes, which are 0.5 mm and 1.5 mm, are adopted in the simulations respectively. Figure 8 shows the instantaneous behavior of the gas–solid two-phase flow in the fluidized bed when the superficial gas velocity is 1.2 m s^{-1} and the particle diameter is 1.5 mm. Compared with Figure 4a, it is obvious that the particles with diameter of 1.5 mm are unable to be fully fluidized at the same gas velocity of 1.2 m s^{-1} in the fluidized bed. The particles are basically packing at the bottom of the bed and only a few large bubbles formed and moving in the upper bed. The time-averaged local solids fraction and heat transfer coefficient around the tube were obtained as shown in Figure 9. Figure 9a presents the distribution of the solids fraction around the tube. Obviously, the solids faction is very high (above 0.5) at the top of the tube, low at the bottom, and reaches a minimum (about 0.2) at the lower part of the left and right sides of the tube. The reason is that a large number of particles are concentrating at the top of the tube almost all the time, as shown in Figure 8. The distribution of the convective heat transfer coefficient between gas and tube around the tube is presented in Figure 9b. It can be seen that the shape of the curve is basically same to that in the fluidized bed with particle diameter of 1 mm, which is shown in Figure 6b. All are ellipse, but the value is low of the range from 50 to 100 W m^{-2} K^{-1}. The distribution of the heat transfer coefficient between particle and tube caused by thermal conduction around the tube is presented in Figure 9c. It can be found that the trend of the curve is similar to that of

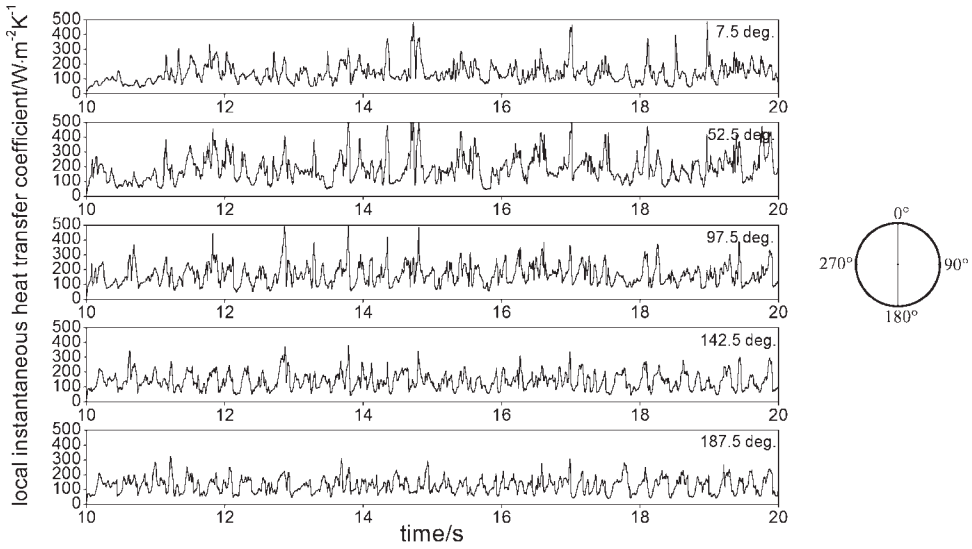

Figure 13. Local instantaneous convective heat transfer coefficient between gas and tube at the different position around the tube in the fluidized bed (u_f = 1.2 m s^{-1}, d_p = 0.5 mm, u_{mf} = 0.24 m s^{-1}).

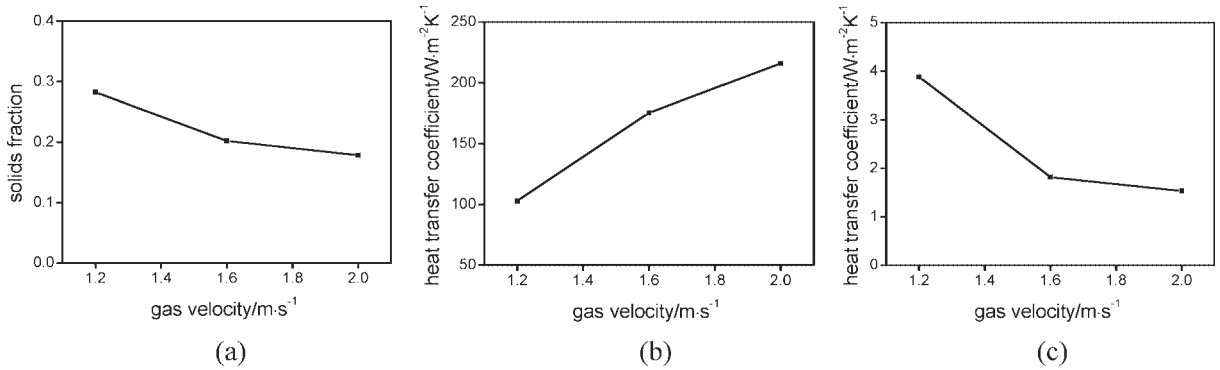

Figure 14. Averaged solids fraction and heat transfer coefficient of the tube in fluidized bed vs. superficial gas velocity (d_p = 1 mm): (a) solids fraction, (b) heat transfer coefficient between gas and tube, (c) heat transfer coefficient between particle and tube.

the distribution curve of the solids fraction in Figure 9a. Although the quantity of the direct contact heat transfer between particle and tube remains very small compared with that of convective heat transfer between gas and tube, is larger more than that in the fluidized bed with particle diameter of 1.0 mm, which is shown in Figure 6c. The reason is that the bigger particles with diameter of 1.5 mm are unable to be fully fluidized at superficial gas velocity of 1.2 m s^{-1}. The solids concentration around the tube is relatively severe and many particles contact with the tube surface for a long time, hence the quantity of heat transfer between particle and tube is relatively larger.

Figure 10 shows the local instantaneous convection heat transfer coefficient between gas and tube at the different position around the tube in the fluidized bed with particle diameter of 1.5 mm. It can be seen that the range of fluctuation of the coefficient is much narrower than that in the fluidized bed with particle diameter of 1.0 mm. This is also due to that the particles with diameter of 1.5 mm can not be fully fluidized in the bed.

Above simulation results illustrate that the increase of particle size has a great effect on the flow pattern and heat transfer efficiency in the fluidized bed. How about the decrease of particle size? Figure 11 shows the instantaneous behavior of the gas–solid two-phase flow when the superficial gas velocity is 1.2 m s^{-1} in the fluidized bed with particle diameter of 0.5 mm. Compared with Figure 4a, it can be found that the gas–solid motion in the fluidized bed with smaller particles is more disordered, and particles can be blown to a higher position at the same superficial gas velocity. The time-averaged solids fraction and heat transfer coefficient around the tube were obtained and investigated to quantitatively study the gas–solids motion and heat transfer behavior in the fluidized bed, as indicated in Figure 12. Figure 12a presents the distribution of solids fraction. It can be seen that the solids fraction is very low at all positions around the tube, all ~0.2, and has a minimum at the slight upper part of the left and right sides of the tube. Particles with diameter of 0.5 mm can be turbulently fluidized at the gas velocity of 1.2 m s^{-1} in the fluidized bed, and there is not any large particle aggregation more around the tube. Figure 12b shows the distribution of convective heat transfer coefficient between gas and tube around the tube. The shape of the curve is also like ellipse. But the value is relatively higher, with a maximum near 200 W m^{-2} K^{-1}. Figure 12c demonstrates the distribution of heat transfer coefficient between particle and tube caused by thermal conduction around the tube, which is somewhat similar to the trend of the distribution of solids fraction indicated in Figure 12a. Compared with the heat transfer between gas and tube, shown in Figure 12b, the quantity of heat transfer caused by direct contact between particles and tube is much smaller,

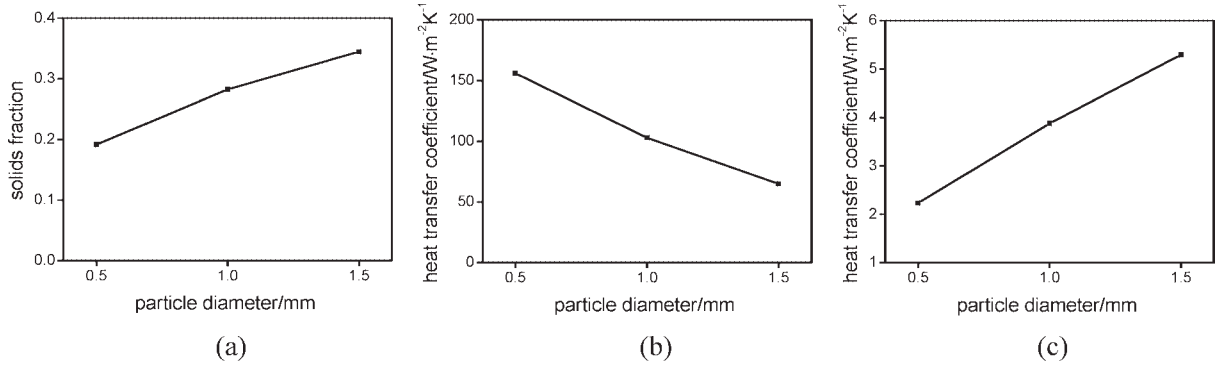

Figure 15. Averaged solids fraction and heat transfer coefficient of the tube in fluidized bed vs. particle diameter (u_f = 1.2 m s^{-1}): (a) solids fraction, (b) heat transfer coefficient between gas and tube, (c) heat transfer coefficient between particle and tube.

$\sim$1% of former. It is also much less than that in fluidized bed with particle diameter of 1.0 mm. The reason is that the particles with diameter of 0.5 mm can not concentrate around the tube when the gas velocity is 1.2 m s^{-1}. Therefore they can't contact with the tube surface for a long time. Hence the quantity of the heat transfer between particle and tube is so small that even can be ignored.

Figure 13 shows the profile of local instantaneous convective heat transfer coefficient between gas and tube around the tube in the fluidized bed with particle diameter of 0.5 mm. It can be seen that the fluctuation of the coefficient is violent, especially at the top and the left and right sides of the tube. This shows that the fluidization in the bed is in turbulent state. By comparing Figures 5b, 10, and 13, it can be found that the intensities of the fluctuation of heat transfer coefficients between gas and tube differ greatly in the fluidized beds when the particle sizes are different, even the gas velocities are same. More violent fluctuation of the heat transfer coefficient indicates more turbulent fluidization of the mediums in the bed.

To explore the effect of gas velocity and particle size on the heat transfer efficiency of the whole tube, time- and space-averaged solids fractions and heat transfer coefficients around the tube in all the simulation cases were obtained in this article. Figure 14 shows the effect of gas velocity. It can be seen that the solids fraction around the tube decreases and the heat transfer coefficient between gas and tube increases with the increase of the gas velocity, but the slope of the curves gradually reduces. Figure 14c shows the relationship between the gas velocity and the heat transfer coefficient caused by particles-tube thermal conduction. It can be found that the heat transfer coefficient gradually decreases as gas velocity rises. By comparing Figures 14b,c, it can be found that the overall heat transfer of the tube is determined by the heat transfer between gas and tube, and the thermal conduction between particles and the tube can be ignored. The total heat transfer coefficient of the tube increases with the increase of the gas velocity, but the extent of increase reduces. This is in agreement with the experimental results.[4,5,6] Figure 15 shows the variations of average solids fraction and heat transfer coefficients with particle size. It can be found that the solids fraction around the tube increases, the convective heat transfer coefficient between gas and tube decreases, and the heat transfer coefficient caused by particles-tube thermal conduction increases with the increase of particle size. The total heat transfer of the tube is still determined by gas-tube heat transfer, and it decreases with the increase of particle size. This is also consistent with the experimental results.[38,39] The agreement of computational and experimental results show that the model established in this article can accurately predict the average heat transfer coefficient under different operating conditions. And the new modified CFD-DEM coupling method can be used to investigate the mechanism of flow and heat transfer in gas–solid fluidized bed or solve some engineering problems in chemical industry.

Conclusions

A new modified CFD-DEM coupling method is established and employed to simulate the flow and heat transfer behavior in the fluidized bed with an immersed tube. Heat transfer mechanism in fluidized bed was explored in microscale. The effect of superficial gas velocity, particles diameter, and other parameters on the heat transfer coefficient around the immersed tube was discussed. Some conclusions are derived as follows:

(1) The new modified CFD-DEM coupling method can accurately predict the flow and heat transfer behavior in the fluidized bed. It is an effective tool to simulate the dense gas–solid two-phase flows in the equipment with complex geometry;

(2) The profile of time-averaged heat transfer coefficient around the tube in the fluidized bed likes ellipse. It is low at the top and bottom, and high at the left and right sides of the tube. And the minimum is approximately 70–80% of the maximum;

(3) The gas–solid flow pattern in the fluidized bed has a great effect on the heat transfer efficiency of the tube. And it is the reason for the ellipse-like distribution of the heat transfer coefficient around the tube;

(4) The gas velocity and the turbulence intensity around the tube have a great effect on the heat transfer between gas and tube. Whereas, the heat transfer caused by thermal conductivity between particles and the tube is mainly related to the solids fraction around the tube;

(5) For glass materials with small thermal conductivity, the contact heat transfer between particles and tube is much weaker than the convective heat transfer between gas and tube, and can be ignored. The heat transfer between the tube and mediums in the bed is mainly completed by fluid convection and particle convection;

(6) The overall heat transfer coefficient of the tube increases with the increase of the gas velocity, and decreases with the increase of particle size.

Acknowledgments

This research is financially supported by the National Basic Research Program of China (Grant No. 2007CB209706) and the Foundation for the Excellent Youthful Teacher of Zhejiang University.

Literature Cited

1. George AH, Smalley JL. An instrumented cylinder for the measurement of instantaneous local heat flux in high temperature beds. *Int J Heat Mass Transfer*. 1991;34:3025–3036.
2. Khan T, Turton R. The measurement of instantaneous heat transfer coefficient around the circumference of a tube immersed in a high temperature fluidized bed. *Int J Heat Mass Transfer*. 1992;35:3397–3406.
3. McKain DL, Clark NN, Atkinson C, Turton R. Correlating local tube surface heat transfer with bubble presence in a fluidized bed. *Powder Technol*. 1994;79:69–81.
4. Sunderesan SR, Clark NN. Local heat transfer coefficients on the circumference of a tube in a gas fluidized bed. *Int J Multiphase Flow*. 1995;21:1003–1024.
5. Kim SW, Ahn JY, Kim SD, Lee DH. Heat transfer and bubble characteristics in a fluidized bed with immersed horizontal tube bundle. *Int J Heat Mass Transfer*. 2003;46:399–409.
6. Wong YS, Seville JPK. Single-particle motion and heat transfer in fluidized beds. *AIChE J*. 2006;52:4099–4109.
7. Gidaspow D. *Multiphase Flow and Fluidization: Continuum and Kinetic Theory Descriptions*. Boston: Academic Press, 1994.
8. Schmidt A, Renz U. Eulerian computation of heat transfer in fluidized beds. *Chem Eng Sci*. 1999;54:5515–5522.

9. He Y, Lu H, Sun Q, Yang L, Zhao Y, Gidaspow D, Bouillard J. Hydrodynamics of gas–solid flow around immersed tubes in bubbling fluidized beds. *Powder Technol*. 2004;145:88–105.
10. Schmidt A, Renz U. Numerical prediction of heat transfer in fluidized beds by a kinetic theory of granular flows. *Int J Therm Sci*. 2000;39:871–885.
11. Schmidt A, Renz U. Numerical prediction of heat transfer between a bubbling fluidized bed and an immersed tube bundle. *Heat Mass Transfer*. 2005;41:257–270.
12. Cundall PA, Strack ODL. A discrete numerical model for granular assemblies. *Geotechnique*. 1979;29:47–65.
13. Tsuji Y, Kawaguchi T, Tanaka T. Discrete particle simulation of two dimensional fluidized bed. *Powder Technol*. 1993;77:79–87.
14. Hoomans BPB, Kuipers JAM, Briels WJ, van Swaaij WPM. Discrete particle simulation of bubble and slug formation in a two-dimensional gas-fluidized bed: a hard sphere approach. *Chem Eng Sci*. 1996;51:99–118.
15. Xu BH, Yu AB. Numerical simulation of the gas-particle flow in a fluidized bed by combining discrete particle method with computational fluid dynamics. *Chem Eng Sci*. 1997;52:2785–2809.
16. Zhou H, Flamant G, Gauthier D, Flitris Y. Simulation of cola combustion in a bubbling fluidized bed by distinct element method. *Chem Eng Res Design*. 2003;81:1144–1149.
17. Li JT, Mason DJ. A computational investigation of transient heat transfer in pneumatic transport of granular particles. *Powder Technol*. 2000;112:273–282.
18. Zhou ZY, Yu AB. Particle scale study of heat transfer in packed and bubbling fluidized beds. *AIChE J*. 2009;55:868–884.
19. Rong D, Mikami T, Horio M. Particle and bubble movements around tubes immersed in fluidized beds—a numerical study. *Chem Eng Sci*. 1999;54:5737–5754.
20. Rong D, Horio M. Behavior of particles and bubbles around immersed tubes in a fluidized bed at high temperature and pressure: a DEM simulation. *Int J Multiphase Flow*. 2001;27:89–105.
21. Iwashita K, Oda M. Rolling resistance at contacts in simulation of shear band development by DEM. *J Eng Mech*. 1998;124:285–292.
22. Ting JM, Corkum BT. Computational laboratory for discrete element geomechanics. *J Comput Civil Eng*. 1992;6:129–146.
23. Sun J, Chen MM. A theoretical analysis of heat transfer due to particle impact. *Int J Heat Mass Transfer*. 1988;31:969–975.
24. Liu A, Liu S. Theoretical study on impact heat transfer between particles in fluidized bed. *Proc CSEE*. 2003;23:161–165.
25. Yovanovich MM. Thermal contact resistance across elastically deformed spheres. *J Spacecraft Rockets*. 1967;4:119–121.
26. Holm R. *Electrical Contacts: Theory and Application*. New York: Springer-Verlag, 1967.
27. Batchelor GK, O'Brien RW. Thermal or electrical conduction through a granular material. *Proc R Soc Lond*. 1977;355:313–333.
28. Watson LV, McCarthy JJ. Heat conduction in granular materials. *AIChE J*. 2001;47:1052–1059.
29. Di Felice R. The voidage function for fluid-particle interaction systems. *Int J Multiphase Flow*. 1994;20:153–159.
30. Ranz WE. Friction and transfer coefficients for single particles and packed beds. *Chem Eng Prog*. 1952;48:247–253.
31. Iwai T, Hong CW, Greil P. Fast particle pair detection algorithms for particle simulations. *Int J Modern Phys C*. 1999;10:823–837.
32. Patankar SV. *Numerical Heat Transfer and Fluid Flow*. Washington DC: Hemisphere, 1980.
33. Van Doormal JP, Raithby GD. Enhancements of the SIMPLE method for predicting incompressible fluid flow. *Numerical Heat Transfer*. 1984;7:147–163.
34. Leonard BP. A stable and accurate convective modeling procedure based on quadratic upstream interpolation. *Computer Methods Appl Mech Eng*. 1979;19:59–98.
35. Wen CY, Yu YH. A generalized method for predicting the minimum fluidization velocity. *AIChE J*. 1966;12:610–612.
36. Glass DH, Harrison D. Flow patterns near a solid obstacle in a fluidized bed. *Chem Eng Sci*. 1964;19:1001–1002.
37. Sitnai O, Whitehead AB. Immersed tubes and other internals. In: Davidson JF, Clift R, Harrison D, editors. *Fluidization*, 2nd ed. New York: Academic Press, 1985; Chapter 14:473–493.
38. Figliola KS, Suarez EG, Pitts DR. Mixed particle size distribution effects on heat transfer in a fluidized bed. *J Heat Transfer*. 1986; 108:913–915.
39. Biyikli S, Chen JC. Effect of mixed particle size on local heat transfer coefficient around a horizontal tube in fluidized beds. In: *Proceedings of the 7th International Heat Transfer Conference*, Munich, Germany, 1982, pp. 39–44.

Manuscript received Oct. 28, 2008, and revision received Apr. 27, 2009.